Optical Engineering

OpticalEngineering.SPIEDigitalLibrary.org

Enhanced sensitivity of heterocore structure surface plasmon resonance sensors based on local microstructures

Wenjie Zhu
Qing Huang
Yong Wang
Elfed Lewis
Minghong Yang

SPIE.

Wenjie Zhu, Qing Huang, Yong Wang, Elfed Lewis, Minghong Yang, "Enhanced sensitivity of heterocore structure surface plasmon resonance sensors based on local microstructures," *Opt. Eng.* **57**(7), 076105 (2018), doi: 10.1117/1.OE.57.7.076105.

Downloaded From: https://www.spiedigitallibrary.org/journals/Optical-Engineering on 12/27/2018
Terms of Use: https://www.spiedigitallibrary.org/terms-of-use

Enhanced sensitivity of heterocore structure surface plasmon resonance sensors based on local microstructures

Wenjie Zhu,[a] Qing Huang,[a] Yong Wang,[a] Elfed Lewis,[b] and Minghong Yang[a,*]
[a]Wuhan University of Technology, National Engineering Laboratory for Fiber Optics Sensing Technology, Wuhan, China
[b]University of Limerick, Optical Fibre Sensors Research Centre, Castletroy, Limerick, Ireland

Abstract. A method to improve the refractive index (RI) and temperature sensitivities of optical fiber based on surface plasmon resonance (SPR) sensors is proposed and experimentally demonstrated. It is realized by using a precision femtosecond laser system to manufacture microstructures on a heterocore optical fiber structure (multimode single-mode multimode fiber, MSM). The microstructured MSM structure fiber-optic sensors were coated with 60-nm gold (Au) film to test and verify RI sensing, obtaining an enhancement of the maximum sensitivity range from 2845.18 to 3313.15 nm/RIU. The fabricated sensors were additionally coated with a layer of polydimethylsiloxane, which has a high negative thermos-optic coefficient, to conduct a series of temperature sensing experiments. Experimental results showed that the maximum sensitivity increased from 1.1998 to 1.5646 nm/°C. Compared with nonmicrostructured sensors, the RI and temperature sensitivity of the proposed sensor has increased 16.4% and 30.2%, respectively. The simply fabricated, low-cost, and high-sensitivity SPR sensor has promising applications in many areas, especially in the biochemical field. © *2018 Society of Photo-Optical Instrumentation Engineers (SPIE)* [DOI: 10.1117/1.OE.57.7.076105]

Keywords: heterocore structure; surface plasmon resonance; femtosecond laser; microstructures; refractive index and temperature sensing.

Paper 180376 received Mar. 11, 2018; accepted for publication Jun. 25, 2018; published online Jul. 25, 2018.

1 Introduction

In the last decades, surface plasmon resonance (SPR) sensors have attracted intensive attention and primarily due to their relatively high sensitivity and short response time.[1,2] They have, therefore, found applications in many fields, including environmental protection, biotechnology, medical diagnostics, drug screening, food safety, industrial materials selection and security.[3–5] The sensing mechanism of SPR sensors is based on the change of external refractive index (RI) of the sensing region when the surrounding medium in close proximity to the waveguide boundary interacts with evanescent field therein generated by the incident light within the waveguide. RI is one of the most basic physical quantities, which facilitates measurement using SPR sensing technology, and almost all the measurands rely on the external RI changes.[6] Conventional SPR sensors based on the traditional Otto or Kretschmann configuration prism-type SPR sensors cannot realize remote and real-time monitoring due to their physical configurations, primarily due to their relatively large size that prohibits their use in applications where space is limited and miniaturization is essential.[7–9] To solve this problem, optical fiber sensors have received increased attention owing to their advantages of potential for relatively high sensitivity, resistance to corrosion, immunity to electromagnetic interference, compact size, and low cost of fabrication.[10–12]

Recently, optical fiber-based SPR sensors with different structures have been proposed, such as tapered fiber,[13] tilted fiber Bragg gratings,[14] long period gratings,[15] and fiber-optic interferometers including Fabry–Perot interferometers.[16] These sensors are high cost and hard to fabricate, and hence recently, heterocore structure optical fiber sensors have been investigated to develop SPR sensors based on relatively simple structures.[17–19] In contrast to the more conventional techniques referred to above, the heterocore structured optical fiber sensor is proved to have potential practicability and several advantages, e.g., acidity measurements.[20] The practical characteristic of this sensor can be found in its simple structure and relatively easy fabrication, which can attain the required appropriate light leakage into the cladding layer, so that the cladding surface is the sensing area. It has already been demonstrated that such SPR sensors have relatively high-sensitivity coupled with good reliability and mechanical strength, which make them ideal candidates for use in the target application areas of this work, such as biochemical field.[21] There are many methods to enhance the sensitivity of sensors, such as chemical etching and side-polishing;[22,23] however, chemical etching will destroy the flexibility of optical fibers, and the operation and accuracy of side-polish technique are hard to control.

In this paper, an entirely new sensor structure based on heterocore structure (multimode singlemode multimode fiber structure, MSM) SPR sensor is described to improve the sensitivity beyond that of existing conventional structured sensors. The high accuracy and fast processing capabilities of

*Address all correspondence to: Minghong Yang, E-mail: minghong.yang@whut.edu.cn

0091-3286/2018/$25.00 © 2018 SPIE

Downloaded From: https://www.spiedigitallibrary.org/journals/Optical-Engineering on 12/27/2018
Terms of Use: https://www.spiedigitallibrary.org/terms-of-use

inhouse femtosecond laser micromachining systems have been accessed[24–27] to produce a series of sensors by manufacturing local microstructures on the cladding of MSM optical fiber structure. A gold (Au) film was subsequently deposited on the surface of processed sensors to facilitate the SPR capability of the sensors. Several experiments have been conducted varying RI and temperature to fully characterize the sensors of this investigation against these parameters. It is shown that compared with the sensor without microstructures, the sensitivities of the micromachined sensors of this investigation exhibit improved performance. Significantly, it is also demonstrated that the sensors of this investigation maintained excellent mechanical strength that facilitates their use in a wide range of practical biochemical applications.

2 Sensing Mechanism

The sensing mechanism of heterocore structure SPR sensor of this investigation can be divided into two parts.

2.1 *Heterocore Structured Optical Fiber Surface Plasmon Resonance Sensor*

The heterocore structure comprises two multimode optical fibers (MMF) and a single-mode optical fiber (SMF), which forms the classical MSM heterocore structure. In detail, a 15-mm length of SMF, whose polyimide layer had been mechanically stripped, was inserted between the two MMF, which serves as the sensing region. The core diameter of the SMF is significantly smaller than that of MMF. The MMF sections simply serve as input and output light waveguide to the sensitive SMF. Therefore, most of the coupled light wave leaks into the cladding layer of the SMF at the input interface of the heterocore region. Such light leakage generates a significant evanescent field when reflecting at the boundary surface between the cladding and the surrounding environment. To induce SPR, a 60-nm-thin layer of Au was deposited around the surface of cladding as shown in Fig. 1.

When the transmitted light wave leaks into the heterocore region, it undergoes total internal reflection at the boundary of the cladding and the Au layer, where the evanescent field is generated and this reaches to the surrounding medium. The excitation condition for the SPR is that the wave vector of the propagation constant of evanescent wave exactly matches with that of the surface plasmon of similar frequency (wavelength) and state of polarization. The corresponding resonance condition for surface plasmons is given as[12]

$$\frac{\omega}{c}\sqrt{\varepsilon_p}\,\mathrm{Sin}\,\theta = \frac{\omega}{c}\sqrt{\left(\frac{\varepsilon_m \varepsilon_s}{\varepsilon_m + \varepsilon_s}\right)}, \tag{1}$$

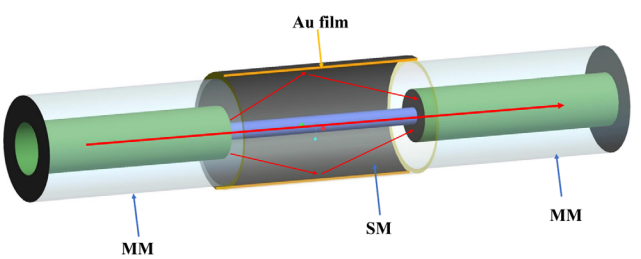

Fig. 1 Heterocore structured SPR sensor.

where ε_m and ε_s represent the dielectric constants of metal layer and the dielectric medium, while ε_p represent the prism dielectric constant (i.e., dielectric constant of cladding in the heterocore structured SPR sensor), ω represents the frequency of incident light, and c is the velocity of light.

2.2 *Femtosecond Laser Machined Structure for Enhanced Surface Plasmon Resonance Effect*

The micromachining process on the cladding surface of the SMF increases the superficial area of the sensing region, which correspondingly increases the light-matter interaction area and hence the sensitivity of the sensor. The schematic profile diagram of the nonmicrostructured sensor and microstructured sensor is shown in Fig. 2.

A_1 is defined as the superficial area of the cylindrical sensing region without microstructures, which is calculated as

$$A_1 = \pi(D + 2m)l, \tag{2}$$

where D is the diameter of cladding layer, m is the thickness of Au film, and l is the length of sensing region.

Treatment using the femtosecond laser allows the formation of microtrenches on the cladding surface (Fig. 2), and the superficial area of microstructured sensing region is calculated as

$$A_2 \approx [\pi(D + 2m) - nw + 2nkd]l, \tag{3}$$

where n is the number of microtrenches, w is the width of microtrenches, and k is a coefficient related to the microstructures. For microtrenches in this investigation, k approximately equals 1. d is the side length of the microtrenches, and d is calculated as

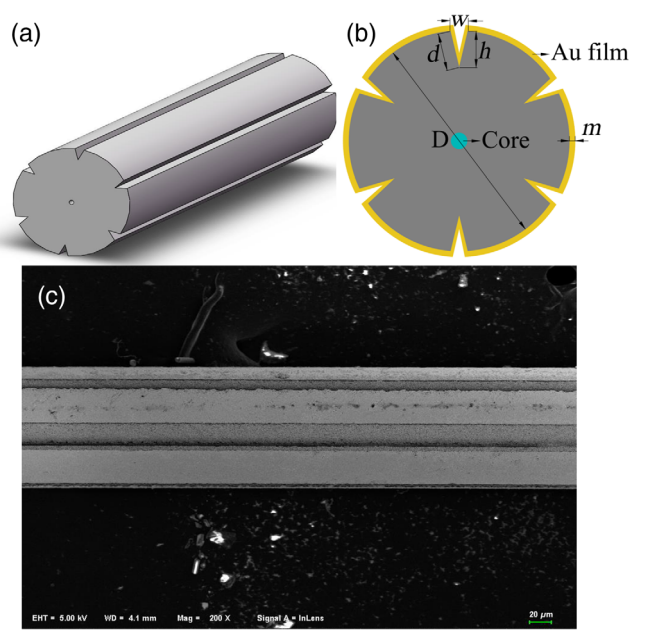

Fig. 2 (a) The schematic profile diagram of the microstructured single-mode fiber, (b) cross section of the sensing region, and (c) SEM image of fabricated sensor.

Downloaded From: https://www.spiedigitallibrary.org/journals/Optical-Engineering on 12/27/2018
Terms of Use: https://www.spiedigitallibrary.org/terms-of-use

$$d \approx \sqrt{\left(\frac{w}{2}\right)^2 + h^2}, \tag{4}$$

where h is the depth of trenches, it is related to the power of femtosecond laser.

3 Device Fabrication and Experiments

3.1 *Heterocore Structured Surface Plasmon Resonance Sensor Fabrication*

The SPR effect is confined to the middle part of heterocore structure, which corresponds to the length of the SMF that is coated by the Au layer. The heterocore structure was fabricated simply using a fusion splicer (FSM-60s by Fujikura) the MMF (core diameter 62.5 μm, cladding diameter 125 μm) and the SMF (core diameter 9 μm, cladding diameter 125 μm). To choose the two kinds of optical fibers, the cost and the convenience were taken into account. The cost of standard optical fibers is relatively low compared with those special fibers and the MMF (62.5/125) and SMF (9/125) are widely used in optical communications, which makes the sensor (MSM) we proposed in the paper have potential applications in industries. First, polyimide layer of the MMF was mechanically stripped and the fiber was then cleaned using ethanol to remove remnant polyimide material and dust. Second, the MMF was accurately cleaved using a fiber cleaver (CT-30 by Fujikura) to allow an 8-mm length available for subsequent fusion splicing. One end of the SMF was processed the same way, but the length was set to be longer than 15 mm. The processed MMF and SMF were fused together and the semimanufactured structure was cleaved at the free end of the SMF leaving the length of SMF to be 15 mm. Finally, another MMF was processed in the identical manner as in the previous case and was then fused at the end of the SMF.

The aim of fabricating the structure in this manner is to optimize the light leakage in cladding layer of the SMF to promote the sensitivity of the heterocore SPR sensor while maintaining adequate light transmission through the structure (i.e., minimizing losses). The new sensor structure has been designed to maximize the superficial area of the sensing region and at the same time enhancing the evanescent field in the sensing region.

3.2 *Microstructures Manufacturing*

To fabricate the local microstructure features on the SMF cladding as straight-trenches, the femtosecond laser precision micromachining system was applied. The femtosecond laser processing system includes an IFRIT laser (wavelength at 780 nm, pulse duration of 180 fs, repetition rate of 1 kHz), a three-dimensional (3-D) table, a beam delivery system (including shutter, attenuator, and aperture), and a CCD monitoring system, as shown in Fig. 3. The sensing region (the SMF) was fixed into the rotating jig such that the fiber rotates with the jig using a precisely controlled stepper motor.

Different microstructures on the surface of the heterocore fiber have been produced by changing the laser parameters. The sample machining parameters are shown in Table 1.

The laser power and the number of trenches can be adjusted, whereas other parameters (machining length, spinning velocity of the rotating jig, and the velocity of stepper motor actuator) are kept the same. To prevent the fabricated sensors from being fragile, the laser power was controlled to the appropriate value using an optical attenuator, which allowed only 11% of the beam energy to be transmitted. It has been experimentally determined that 6 mW is the minimum laser power required to ablate the cladding of optical fiber. In this investigation, the maximum laser power was 20 mW, which ensured that an adequate depth of microtrench obtained adequate mechanical strength.

The number of trenches on the sensing region was controlled using the stepper motor. For one trench, the femtosecond laser ablated the fiber only once with the stepper motor motionless during the machining process. For three trenches, the stepper motor rotated one-third of a circle each time after the femtosecond laser ablated the fiber. For six trenches (the maximum number made), it was one-sixth.

Laser produces fiber debris in the microtrenches, which results in a potentially roughened surface. To remove the

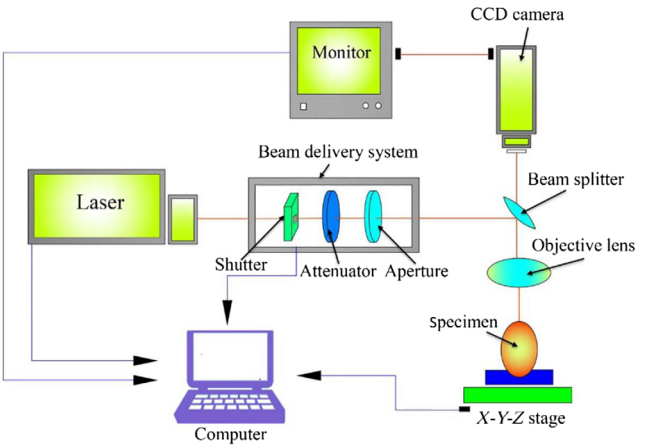

Fig. 3 The diagrammatic sketch of femtosecond laser micromachining system.

Table 1 The parameters of sensors.

Sample No.	Laser power (mW)	Number of trenches
1#	0	0
2#	0	0
3#	10	1
4#	15	1
5#	20	1
6#	10	3
7#	15	3
8#	20	3
9#	10	6
10#	15	6
11#	20	6

Downloaded From: https://www.spiedigitallibrary.org/journals/Optical-Engineering on 12/27/2018
Terms of Use: https://www.spiedigitallibrary.org/terms-of-use

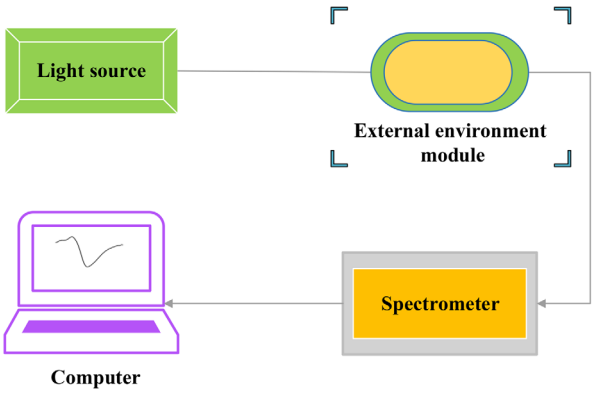

Fig. 4 Experimental setup diagrammatic sketch of the heterocore microstructured SPR RI-sensing system.

debris produced during the process, the samples were cleaned in 2% HF for 2 min and then cleaned using deionized (DI) water. Following the cleaning treatment, a 60-nm Au film was coated on the surface of microstructured sensor using magnetron sputtering technique. The parameters of magnetron sputtering system were precisely controlled to obtain the same thickness of gold film in order not to affect the properties of the sensors.

3.3 *Refractive Index Sensing*

For this new type of SPR sensor, a series of glycerol-water solutions with different concentrations from 0% to 45% was prepared. The RI differs from 1.3330 to 1.3931. The schematic diagram of the experimental system is shown in Fig. 4, including a Tungsten Halogen light source (HL-2000 manufactured by Ocean Optics), a spectrometer (FLAME-S manufactured by Ocean Optics), an external environment module (for RI measurements, the water-glycerol solution), and a laptop computer with running a software developed by Ocean Optics. Eleven samples were prepared in total. Two of them were used in conjunction with a heterocore structured sensor without microstructures (sample 1# and sample 2#). All the sensors exhibited good sensitivity in the experiments.

3.4 *Temperature Sensing*

For temperature sensing, a layer of polydimethylsiloxane (PDMS) was coated on the fabricated SPR sensors by dropping it on the sensors. Then, the samples were placed in a drying oven with the temperature at 120°C for 1.5 h to cure. With this process, the sensors were successfully coated with PDMS, and the temperature sensors were fabricated. The addition of the PDMS coating also provides the sensor with additional strength.

Following fabrication, the temperature sensor was placed in a temperature controller (Electrothermal Forced Air Convection Drying Oven 101-1AB by CHINA TAISITE Instrument). We set a series of temperatures from 50°C to 120°C, with one step every 10°C. The testing system is similar to the RI sensing system (the difference being the external environment is a temperature controller), the experimental setup is shown in Fig. 5.

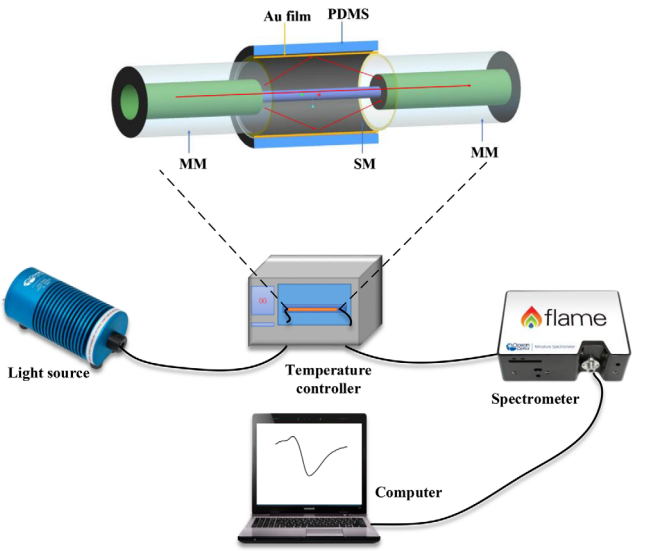

Fig. 5 Experimental setup of the heterocore microstructured SPR temperature-sensing system.

4 Results and Discussion

The transmission spectrum of the sensors was monitored using the broadband light source and spectrometer as shown in Figs. 4 and 5. For RI sensing, by varying the external RI from 1.3330 to 1.3936, the dip of the spectrum was observed as moving toward longer wavelengths, i.e., a red shift. The transmission spectrum of heterocore microstructured SPR sensor at different RI values is shown in Fig. 6.

To verify the consistency of the RI sensing properties of the basic sensors without microstructured features, two separate MSM SPR sensors were selected (sample 1# and sample 2#) and their RI sensitivities were evaluated. The results are shown in Fig. 7(a).

As shown in Fig. 7, the sensitivity of RI is nonlinear, the sensitivities when RI = 1.3330 and 1.3931, respectively, are listed in Table 2, and an inhouse algorithm was developed to describe the sensitivity of fabricated sensors as the

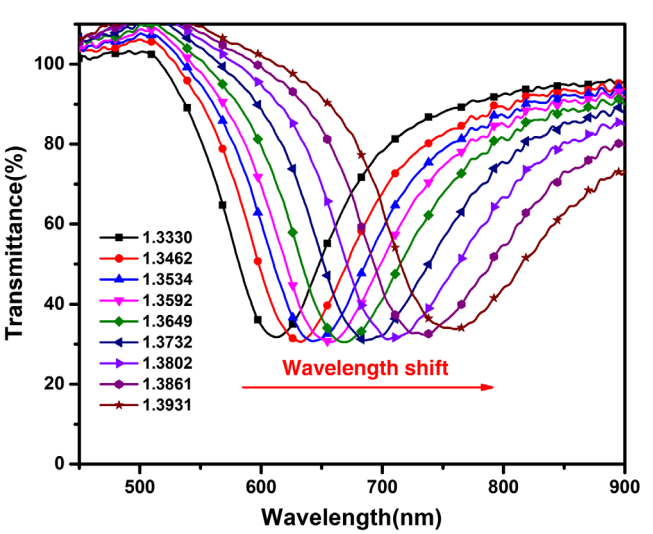

Fig. 6 The transmission spectra of heterocore structure SPR sensors at different RIs.

Downloaded From: https://www.spiedigitallibrary.org/journals/Optical-Engineering on 12/27/2018
Terms of Use: https://www.spiedigitallibrary.org/terms-of-use

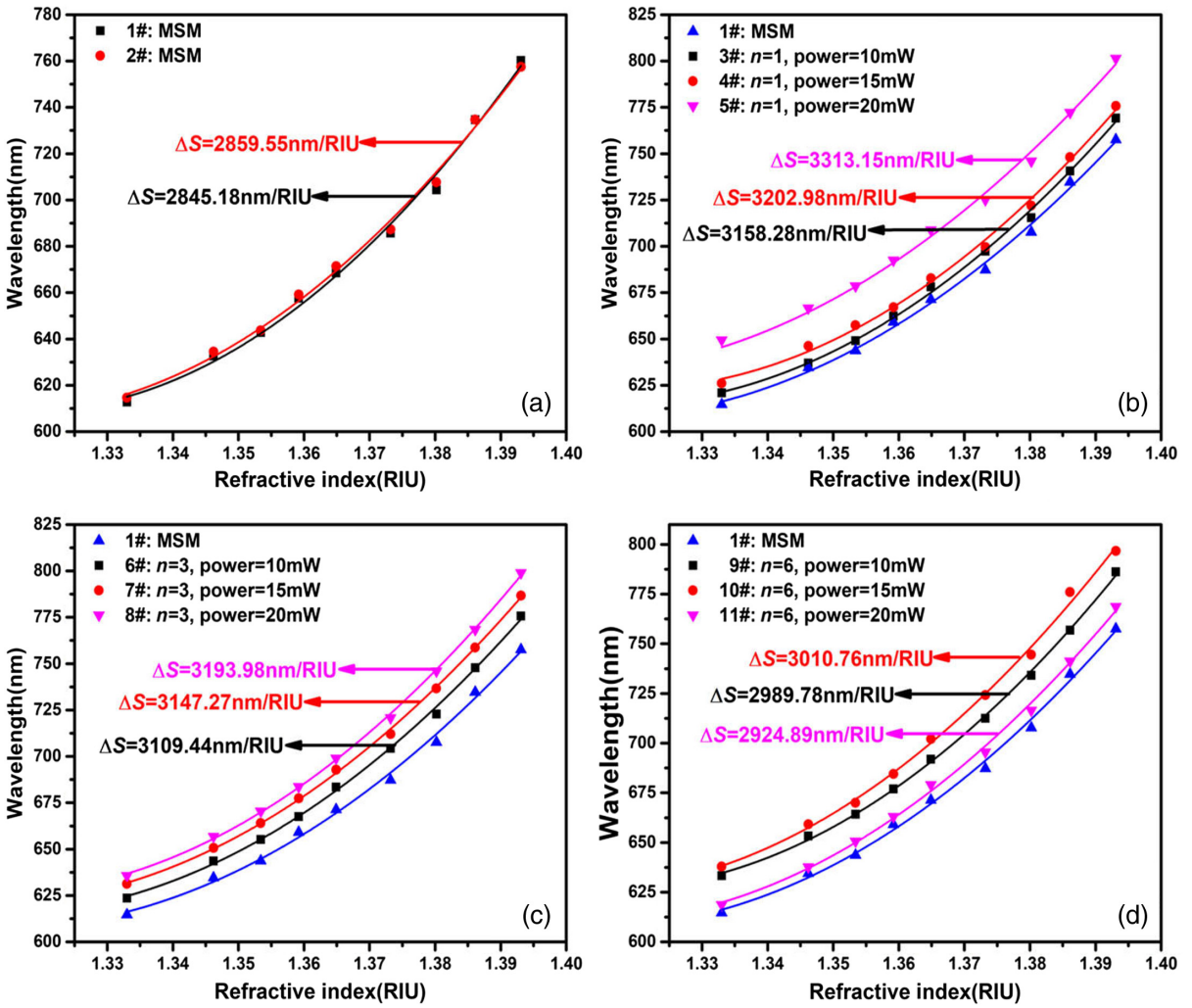

Fig. 7 The sensitivity ranges of fabricated RI sensors: (a) heterocore (MSM) SPR sensors without microstructures, (b) the sensitivity ranges comparisons of one microtrench with nonmicrostructured MSM sensor, (c) the sensitivity ranges' comparisons of three-trenches with nonmicrostructured MSM sensor, and (d) the sensitivity ranges' comparisons of six microtrenches with nonmicrostructured MSM sensor.

Table 2. RI sensitivities of fabricated sensors.

Sample No.	S1.3330 (nm/RIU)	S1.3931 (nm/RIU)	ΔS (nm/RIU)
1#	913.72	3758.91	2845.18
2#	906.34	3765.89	2859.55
3#	935.05	4093.33	3181.38
4#	993.20	4196.18	3202.98
5#	1009.1	4322.25	3313.15
6#	1003.21	4112.65	3109.44
7#	978.37	4065.58	3087.28
8#	871.91	4065.89	3193.98
9#	997.93	3998.93	3001.20
10#	967.90	3978.66	3010.76
11#	980.51	3905.40	2924.89

relationship between external RI and wavelength is nonlinear. ΔS, the sensitivity range, was defined as the sensitivity at 1.3931 minus the sensitivity at 1.3330 was calculated as follows:

$$\Delta S = S_{1.3931} - S_{1.3330}. \tag{5}$$

The results of Fig. 7(a) show that the differences in sensitivity between the two sensors were negligible, in the other words, the differences between different versions of samples coating can be ignored. Figures 7(b), 7(c), and 7(d) show the sensitivities comparisons between microstructured sensors and nonmicrostructured sensor.

The sensitivities of all the sensors are shown in Table 2 and Fig. 7. It is apparent that the microstructured sensors are more sensitive to RI than the nonmicrostructured sensors. It is clear from Fig. 7 that sample 5# has the largest sensitivity range, for which the sensitivity range was 3313.15 nm/RIU. It was also the case that sample 5# ($n = 1$, power $= 20$ mW) has the best response to the changes of external RI among all of the 11 samples. The improvement of sensitivity compared with the unmodified sensors (samples 1# and 2#) was 16.4%

Downloaded From: https://www.spiedigitallibrary.org/journals/Optical-Engineering on 12/27/2018
Terms of Use: https://www.spiedigitallibrary.org/terms-of-use

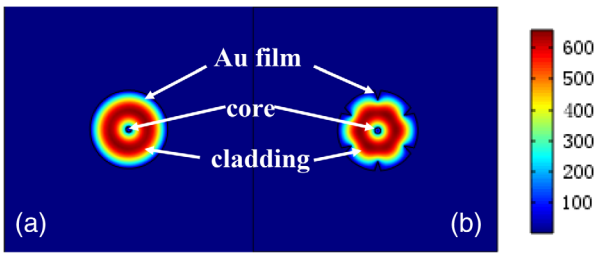

Fig. 8 (a) The mode filed of SMF and (b) the mode filed of microstructured SMF.

and therefore it is clear that the microstructured process has an obvious increase of RI sensitivity. An explanation for the increased sensitivity is that the microstructured sensors have a larger sensing region area that results in a larger light-matter interaction volume and hence the higher sensitivity. Moreover, the sensitivity of the microstructured sensors has been improved in varying degrees.

Figures 8(a) and 8(b) show high-order mode filed simulation results of SMF and microstructured SMF. The simulation results were given by the COMSOL Multiphysics software (version no. 5.1). The shape and the size of the simulation target were set by giving their geometric parameters. The effective refractive indices of the external environment (in this simulation as the air), the SMF-core, the SMF-cladding were set to 1, 1.4679, and 1.4613, respectively. And the RI of gold film was set to $0.63869 + 4.3601i$. As the thickness of the gold film was too thin to effect the mode distribution of the cladding mode, it was neglected in this analysis. The boundary condition was set to perfect electric conductor. The simulation results show that the energy of the cladding mode is more concentrated in a position near the core. However, the energy of cladding mode distributes as RI rings in SMF, whereas in microstructured SMF the energy of cladding mode is concentrated in the vicinity of the microstructures, as shown in Fig. 8(b), which enhances light-matter interacts in the surface of sensing region. Therefore, the effective RI of the microstructured SMF can stimulate a stronger SPR and improve the RI sensitivity of the sensor.

In the case of temperature measurement, PDMS has a high negative thermo-optic coefficient, its RI decreases (increases) as the external temperature increases (decreases). The simplest equation of temperature dependence is the derivative of RI with respect to temperature, i.e., the thermo-optic coefficient. For PDMS at 25°C, it is $\sim -5 \times 10^{-4}$/°C, the functional relationship between temperature and the RI of PDMS is defined as[28]

$$\varepsilon = \frac{\mathrm{d}n}{\mathrm{d}T}, \tag{6}$$

where ε is the thermo-optic coefficient of PDMS, n is the RI of the material, and T is the external temperature. Therefore, when the external temperature changes, the RI of PDMS also changes, which provide an external RI environment for the gold-coated SPR sensors. The thermo-optic coefficient is one of the intrinsic material properties. The temperature sensitivities were estimated by RI changes caused by temperature changes based on Eq. (6), which was defined by the property of PDMS. When the temperature increased between 50°C and 120°C, the transmission spectrum was observed as

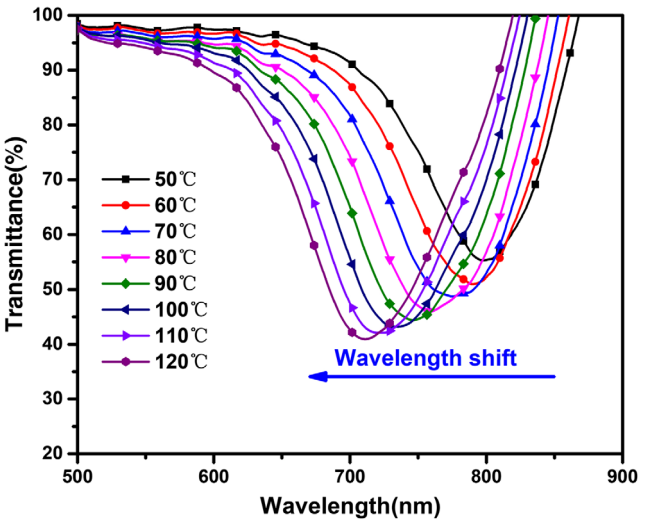

Fig. 9 The transmission spectra of heterocore SPR sensors at different temperatures.

shown in Fig. 9. In this case, as the temperature increases the spectrum exhibits a blue shift and the transmission depth is lower (greater attenuation at the dip value).

As shown in Fig. 10, the relationship between temperature and wavelength shift is linear. Figure 10(a) shows that the two MSM SPR sensors without microstructures (samples 1# and 2#) have almost the same sensitivity. The sensitivities of microstructured sensors were improved in varying degrees with the addition of the microstructured features, as shown in Figs. 10(b), 10(c), and 10(d). Again, it is clear that sample 5# ($n = 1$, power = 20 mW) has the highest sensitivity. By comparison with samples 1# and 2#, the temperature sensitivity increases about 30.2%. This phenomenon can be attributed to the fact that femtosecond laser processing increased the sensing region area of sensors response to external environment. However, the sensitivity is not linearly or even continuously related with an increase in the superficial area. Figure 10 shows the absolute temperature sensitivity of the fabricated device versus the increase in superficial area. The first data point (at 0, 1.20 nm/°C) represents the MSM SPR sensor without any additional microstructures, whose increased superficial area is 0.

From Fig. 11, it is apparent that the temperature sensitivity initially increases to a maximum of 1.5646 nm/°C with the superficial area increasing, but then reaches a sensitivity plateau value of around 1.38 nm/°C beyond the area value of 300 μm^2. The last three data points, therefore, show that the temperature sensitivity reaches a saturated value, beyond which the temperature sensitivity does not increase with an increase in the superficial area. Therefore, in the case that the number of trenches is 6, the power of femtosecond laser is 10, 15, and 20 mW, no increase in sensitivity is observed. It can be explained that with the superficial area increasing, the sensing region expanded, which also expanded the evanescent field. This change was not helpful all the time, it might increase the instability of sensors, resulting in the sensitivity decreased. In the other words, the expansion of the evanescent field is limited due to the property of the heterocore structure (MSM), especially the SMF (the sensing region). In this investigation, the number of microtrenches increase will directly expand the superficial area of the

Downloaded From: https://www.spiedigitallibrary.org/journals/Optical-Engineering on 12/27/2018
Terms of Use: https://www.spiedigitallibrary.org/terms-of-use

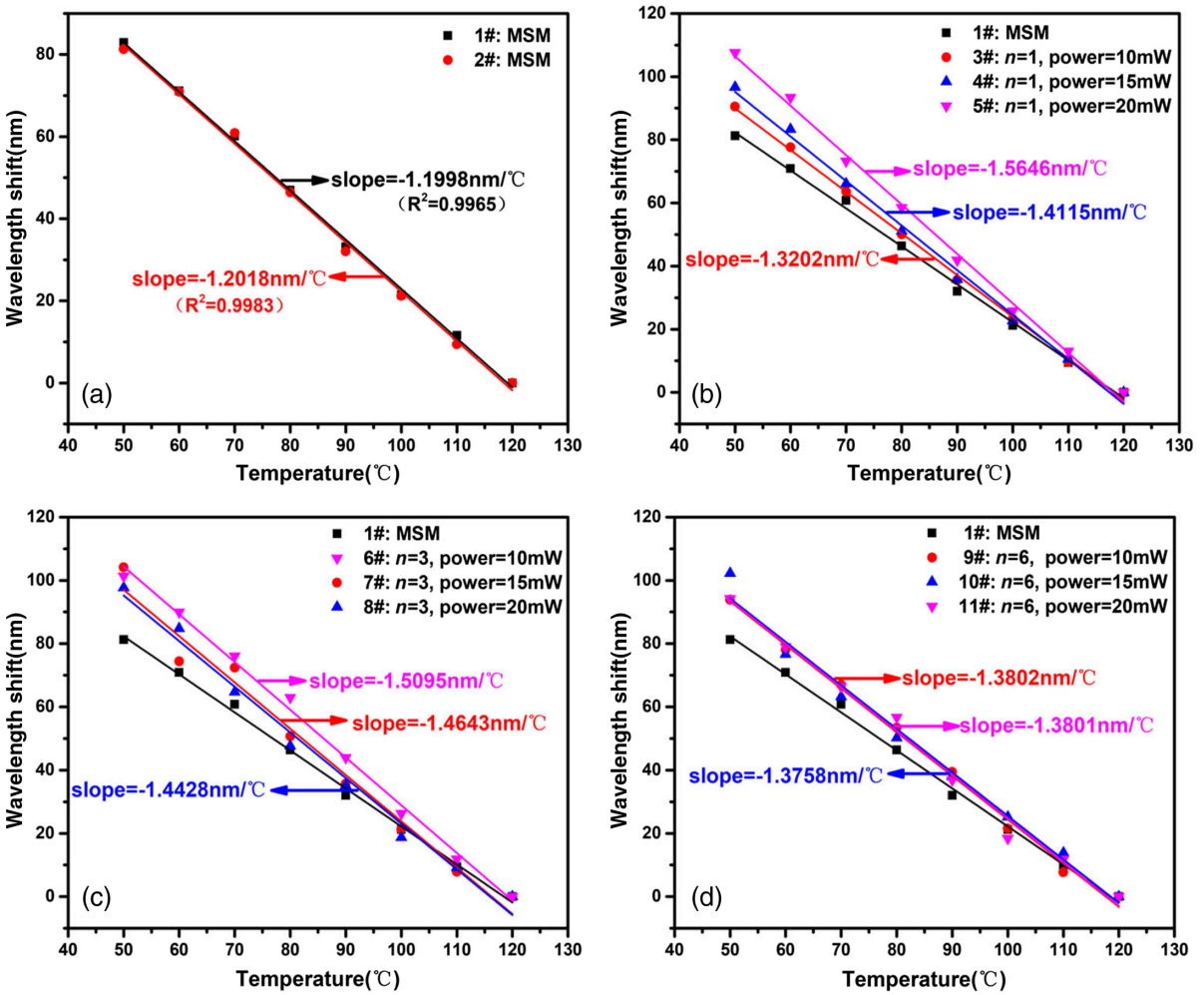

Fig. 10 The temperature sensitivities of fabricated sensors: (a) the sensitivities of MSM SPR temperature sensors, (b) sensitivities comparisons of one microtrench with nonmicrostructured MSM sensor, (c) sensitivities comparisons of three microtrenches with nonmicrostructured MSM sensor, and (d) sensitivities comparisons of six microtrenches with nonmicrostructured MSM sensor.

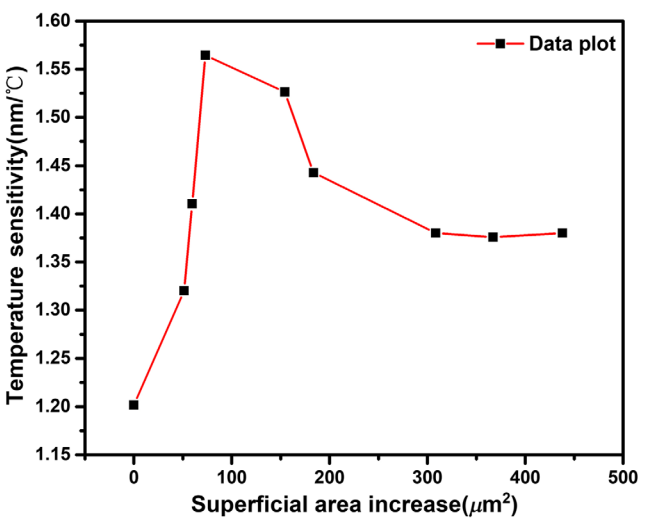

Fig. 11 The relationship between increased superficial area and sensitivities of fabricated sensors for temperature sensing.

sensing region, that is to say, more light leakage occurs through this process. It indeed improves light-matter interacts, but more light leakage would result in less light output, which has negative influences on reaction response time and it has instabilities to external environment changes. Even so, the microstructured MSM SPR sensors still provided higher sensitivity than those without microstructures, the minimum increase reached 14.5%.

5 Conclusion

Sensor configurations have been fabricated on the cladding of conventional MSM optical fiber heterocore structures using a 780-nm femtosecond laser resulting in a new sensor to provide enhanced sensitivity of MSM-SPR combination sensors. Two versions of the sensors have been used to measure RI and temperature. SPR behavior was achieved using a 60-nm-thick gold film sputtered on the sensing region thus forming a microstructured heterocore structure SPR sensor.

In the case of RI measurement, the microstructured sensors exhibit higher sensitivity than the corresponding nonmicrostructured sensors. The number of microtrenches

Downloaded From: https://www.spiedigitallibrary.org/journals/Optical-Engineering on 12/27/2018
Terms of Use: https://www.spiedigitallibrary.org/terms-of-use

and power of the incident laser has a direct influence on the sensing performance. As a result, RI sensitivity can be improved by 16.4%, using a laser power of 20 mW with only one microtrench feature. In the case of temperature sensing, PDMS, a temperature-sensitive material, was coated on the surface of fabricated SPR sensors to study the resulting temperature-sensing properties. Again, the optimum sensitivity was obtained when the number of microtrench was 1 and the laser power was 20 mW. In this case, the temperature sensitivity was 30.2% higher than the corresponding sensor with no microstructured features. Hence, this low-cost, simply fabricated, and highly sensitive microstructured heterocore structure SPR sensor has excellent potential for use in biochemical, industry, and materials selection applications.

Disclosures

The authors declare no conflicts of interests in the article.

Acknowledgments

This work was financially supported by the Project of National Natural Science Foundation of China (NSFC, Project No.: 61575151).

References

1. J. Homola, S. S. Yee, and G. Gauglitz, "Surface plasmon resonance sensors: review," *Sens. Actuators B: Chem.* **54**(1-2), 3–15 (1999).
2. J. Homola and M. Piliarik, "Surface plasmon resonance (SPR) Sensors," **4**, 45–67 (2006).
3. E. Wijaya et al., "Surface plasmon resonance-based biosensors: from the development of different SPR structures to novel surface functionalization strategies," *Curr. Opin. Solid State Mater. Sci.* **15**(5), 208–224 (2011).
4. C. M. Miyazaki, F. M. Shimizu, and M. Ferreira, "Surface Plasmon Resonance (SPR) for Sensors and Biosensors," Chapter 6 in *Nanocharacterization Techniques*, pp. 183–200, Elsevier (2017).
5. C. M. Miyazaki et al., "Surface plasmon resonance biosensor for enzymatic detection of small analytes," *Nanotechnology* **28**(14), 145501 (2017).
6. X. D. Wang and O. S. Wolfbeis, "Fiber-optic chemical sensors and biosensors (2013-2015)," *Anal. Chem.* **88**(1), 203–227 (2016).
7. G. Kaur et al., "Detection of Neisseria meningitidis using surface plasmon resonance based DNA biosensor," *Biosens. Bioelectron.* **78**, 106–110 (2015).
8. J. F. Masson et al., "Dual Kretschmann and Otto configuration fiber surface plasmon resonance biosensor," *Opt. Express* **25**(22), 26950–26957 (2017).
9. X. Yang et al., "Optical property and adsorption isotherm models of glucose sensitive membrane based on prism SPR sensor," *Sens. Actuators B: Chem.* **237**, 150–158 (2016).
10. S. Sharma et al., "A novel method of SPR based SnO 2: GNP nanohybrid decorated optical fiber platform for hexachlorobenzene sensing," *Sens. Actuators B: Chem.* **246**, 927–936 (2017).
11. Y. Zhao, Z. Q. Deng, and H. F. Hu, "Fiber-optic SPR sensor for temperature measurement," *IEEE Trans. Instrum. Meas.* **64**(11), 3099–3104 (2015).
12. A. K. Sharma, R. Jha, and B. D. Gupta, "Fiber-optic sensors based on surface plasmon resonance: a comprehensive review," *IEEE Sens. J.* **7**(8), 1118–1129 (2007).
13. Y. C. Kim et al., "Tapered fiber optic surface plasmon resonance sensor for analyses of vapor and liquid phases," *Opt. Lett.* **30**(17), 2218–2220 (2005).
14. M. D. Baiad and R. Kashyap, "Concatenation of surface plasmon resonance sensors in a single optical fiber using tilted fiber Bragg gratings," *Opt. Lett.* **40**(1), 115–118 (2015).
15. W. Wei et al., "Graphene-based long-period fiber grating surface plasmon resonance sensor for high-sensitivity gas sensing," *Sensors* **17**(1), 2 (2017)..
16. S. Chen et al., "Temperature-compensating fiber-optic surface plasmon resonance biosensor," *IEEE Photonics Technol. Lett.* **28**(2), 213–216 (2015).
17. M. Iga, A. Seki, and K. Watanabe, "Gold thickness dependence of SPR-based hetero-core structured optical fiber sensor," *Sens. Actuators B: Chem.* **106**(1), 363–368 (2005).
18. M. Iga, A. Seki, and K. Watanabe, "Hetero-core structured fiber optic surface plasmon resonance sensor with silver film," *Sens. Actuators B: Chem.* **101**(3), 368–372 (2004).
19. Y. Wang et al., "Novel optical fiber SPR temperature sensor based on MMF-PCF-MMF structure and gold-PDMS film," *Opt. Express* **26**(2), 1910–1917 (2018).
20. M. Iga et al., "Acidity measurements based on a hetero-core structured fiber optic sensor," *Sens. Actuators B: Chem.* **96**(1–2), 234–238 (2003).
21. C. Caucheteur, T. Guo, and J. Albert, "Review of plasmonic fiber optic biochemical sensors: improving the limit of detection," *Anal. Bioanal. Chem.* **407**(14), 3883–3897 (2015).
22. T. Wu et al., "Surface plasmon resonance biosensor based on gold-coated side-polished hexagonal structure photonic crystal fiber," *Opt. Express* **25**(17), 20313–20322 (2017).
23. C. Caucheteur et al., "Hybrid fiber gratings coated with a catalytic sensitive layer for hydrogen sensing in air," *Opt. Express* **16**(21), 16854–16859 (2008).
24. X. Zhou et al., "FBG hydrogen sensor based on spiral microstructure ablated by femtosecond laser," *Sens. Actuators B: Chem.* **236**, 392–398 (2016).
25. M. Zou et al., "Femtosecond laser ablated FBG with composite microstructure for hydrogen sensor application," *Sensors* **16**(12), 2040 (2016).
26. P. Chen et al., "Ultra-sensitive refractive index sensor based on an extremely simple femtosecond-laser-induced structure," *Opt. Lett.* **42**(6), 1157–1160 (2017).
27. E. Bulushev et al., "High-speed and crack-free direct-writing of microchannels on glass by an IR femtosecond laser," *Opt. Lett.* **79**, 39–47 (2016).
28. J. Li et al., "A high sensitivity temperature sensor based on packaged microfibre knot resonator," *Sens. Actuators A: Phys.* **263**, 369–372 (2017).

Wenjie Zhu received his bachelor's degree in materials science and engineering from Wuhan University of Technology, Wuhan, China, in 2016. Now, he is studying for a master's degree at National Engineering Laboratory for Optical Fiber Sensing Technology in Wuhan University of Technology. His research interests are focused on material synthesis and their applications in optical fiber sensing.

Qing Huang received her bachelor's degree in materials physics from Wuhan Institute of Technology, Wuhan, China, in 2013. Now, she is studying for her doctorate in materials science and engineering at National Engineering Laboratory for Optical Fiber Sensing Technology in Wuhan University of Technology. Her research interests are focused on material synthesis and their applications in optical fiber sensing.

Yong Wang received his bachelor's degree in materials science and engineering from Wuhan University of Technology, Wuhan, China, in 2017. Now, he is studying for a master's degree at National Engineering Laboratory for Optical Fiber Sensing Technology in Wuhan University of Technology. His research interests are focused on optical fiber fabrication and optical fiber sensing technology.

Elfed Lewis received his BEng (Hons.) degree in electrical and electronic engineering and his PhD both from Liverpool University, Liverpool, U.K., in 1978 and 1987, respectively. He is an associate professor and the director of the Optical Fiber Sensors Research Centre at University of Limerick, which he founded in 1996, and he is a fellow of the Institute of Physics and IET.

Minghong Yang received his PhD in physics from Huazhong University of Science and Technology, Wuhan, in 2003. In 2003–2005, he worked as a postdoc fellow at the Fraunhofer Institute for Applied Optics and Fine Mechanics in Jena, Germany. In 2006 to 2008, he worked at Berlin University of Technology as a research fellow. He is now a research scientist in the National Engineering Laboratory for Fiber Optic Sensing Technology in the Wuhan University of Technology.

Downloaded From: https://www.spiedigitallibrary.org/journals/Optical-Engineering on 12/27/2018
Terms of Use: https://www.spiedigitallibrary.org/terms-of-use